Enhancement of surface photocurrents in topological insulators using magnetic superlattices

Netanel H. Lindner,[1] Gil Refael,[2] and Felix von Oppen[3]

[1]*Department of Physics, Technion, Haifa 32000, Israel*
[2]*Institute of Quantum Information and Matter, Dept. of Physics, Caltech, Pasadena, CA 91125*
[3]*Dahlem Center for Complex Quantum Systems and Fachbereich Physik, Freie Universität Berlin, 14195 Berlin, Germany*

The gapless surface states of topological insulators (TI) can potentially be used to detect and harvest low-frequency infrared light. Nonetheless, it was shown that significant surface photocurrents due to light with frequency below the bulk gap are rather hard to produce. Here we demonstrate that a periodic magnetic pattern added to the surface dramatically enhances surface photocurrents in TI's . The ability to produce substantial photocurrents on TI surfaces from mid-range and far-infrared light could be used in photovoltaic applications, as well as for detection of micrometer wavelength radiation.

Light-matter interactions are central to modern science and technology. It is the principle at the heart of many solid-state material probes, and at the same time, it is an important ingredient in our energy economy, particularly through photovoltaic harvesting of solar energy. A challenging problem of solar energy is how to harness the infrared (IR) spectrum of the sun, which could increase dramatically solar energy harvesting efficiency. Efforts to extend the spectrum accessible in photovoltaics concentrated on new low band-gap materials; organics [1–4], as well as carbon nanotubes [5–7] were shown capable of IR harvesting, albeit with a small efficiency. Another approach utilizes plasmonics as an intermediate step between IR and currents in a semiconductor [8–10].

When mentioning new materials for IR harversting, topological insulators [11–15] immediately come to mind. On the one hand, they have a unique response to electromagnetic terms, as encoded in their theta term [16–18]. More importantly, their mid-gap surface states with spin-momentum locking raised hopes that circularly-polarized light could easily produce surface photocurrents in them. These hopes have gone unfulfilled. Even when including a series of modifications to the band structure likely to appear in real materials, such as warping, band curvature, or a uniform magnetic field, the photocurrents produced in response to sub-bandgap light were shown to be remarkably minute, even when a high-intensity laser is considered [19, 20]. The only scheme for producing a photo-voltage so far relied on the unique thermoelectric effects associated with a Dirac cone dispersion [21].

In this manuscript we describe how to turn a topological insulator surface with a simple Dirac dispersion into a photocurrent rectifier. We show that by adding a magnetic coating with a spatially periodic magnetic texture, the TI produces a significant photocurrent in response to circularly polarized light in the IR regime. This effect should, in prinicipal, allow making diode-free IR sensitive photocells from topological insulator films. It also enables investigating the unique properties of TI surfaces using non-ionizing light (as in [22]). As we show below, the two dimensional photocurrent density resulting from illumination with sunlight could reach $10^{-7}\frac{A}{m}$. Illumination with a conventional laser beam can yield currents of the order of $10^{-3}\frac{A}{m}$.

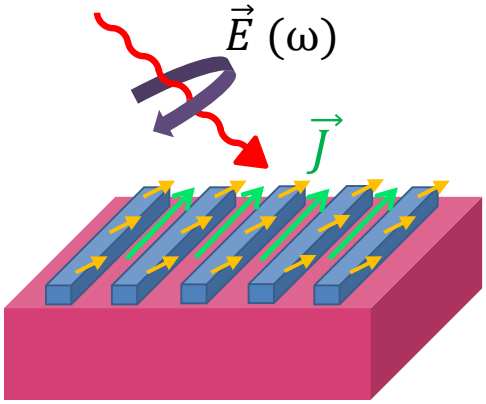

Figure 1: Proposed scheme for achieving a photovoltaic effect on a topological-insulator surface, coated by a magnetic grating. When the magnetization (depicted as yellow arrows) breaks both rotation and reflection symmetries, circularly polarized light induces a photocurrent (green) in the direction parallel to the stripes.

Our photocurrent rectification scheme emerges from the minimal model of a surface of a 3D topological insulator (TI). With the surface lying in the xy plane, the Hamiltonian describing the surface electrons is

$$H_0 \;=\; v_F\left(p_x\sigma^y - p_y\sigma^x\right), \qquad (1)$$

where σ^x, σ^y are Pauli matrices, and $\mathbf{p} = (p_x, p_y) = \left(\frac{\hbar}{i}\frac{\partial}{\partial x}, \frac{\hbar}{i}\frac{\partial}{\partial y}\right)$. This model is clearly time-reversal and rotationally invariant, $\mathcal{T}H_0\mathcal{T}^{-1} = U_\phi H_0 U_\phi^\dagger = H_0$, with the symmetry operators

$$\mathcal{T} = i\sigma_y K, \qquad U_\phi = e^{i\phi(\sigma^z/2 + L_z/\hbar)}. \qquad (2)$$

Here, K denotes complex conjugation, $L_z = xp_y - yp_x$ is the orbital angular momentum normal to the surface, and ϕ the angle of rotation.

These two symmetries immediately imply no current response to incident light. Time-reversal invariance requires that the incident beam is circularly polarized to see any response. Since circularly polarized light, however, has no preferred direction on the surface, the rotational symmetry rules out any net photocurrent from forming. In materials such as Bi_3Se_2, the lattice structure reduces the full $SO(2)$ rotational symmetry to a C_3 symmetry, with $\phi = 2\pi/3$ in Eq. (2). This allows H_0 to have a trigonal warping term [23]. However even with the reduced symmetry, no photocurrents are possible [19, 20].

Next, we consider a magnetic grating structure deposited on the surface, see Fig. 1. Consider strips of a ferromagnetic material set parallel to the y axis, and placed periodically with a wave number $\mathbf{q} = (q, 0)$. We model the proximity-induced ferromagnetic interaction on the surface electrons by

$$V = \mathbf{u} \cdot \boldsymbol{\sigma} \cos(qx). \tag{3}$$

Once the magnetic structure is introduced, it is convenient to enumerate the eigenstates of the full Hamiltonian, $H = H_0 + V$ within the reduced Brillouin zone (BZ) in terms of the quasi-momentum $k_x \in [-\frac{q}{2}, \frac{q}{2}]$ in x-direction, using Greek indices to denote the bands. Thus denote the eigenstates as $|k_x, k_y; \alpha\rangle$. We use the convention that conduction bands are enumerated by $\alpha > 0$ and valence bands by $\alpha < 0$, as illustrated in Fig. 2

The addition of the magnetic strips on the surface alters its symmetries. Time-reversal symmetry remains, as long as we consider a modified operator: $\tilde{\mathcal{T}} = \mathcal{T}M$ with $MxM^\dagger = x + \pi/q$. The eigenstates and energies transform as

$$|-k_x, -k_y; \alpha\rangle = \tilde{\mathcal{T}} \, |k_x, k_y; \alpha\rangle \, , E_{-k_x,-k_y;\alpha} = E_{k_x,k_y;\alpha} \tag{4}$$

Particle-hole symmetry is also present. First define Π_a as the spatial reflection operator about the $a = x, y$ directions, e.g., $\Pi_x x \Pi_x = -x$. Now, $\mathcal{C} = \Pi_x \Pi_y \mathcal{T}$ implements:

$$|k_x, k_y; -\alpha\rangle = \mathcal{C} \, |k_x, k_y; \alpha\rangle \, , E_{k_x,k_y;\alpha} = -E_{k_x,k_y;-\alpha}. \tag{5}$$

Additional symmetries appear restricted due to the arbitrary form of V.

Nonetheless, a gauge transformation allows us to cancel an arbitrary u_y component of V, and allows additional mirror symmetries. Define the gauge transformation

$$G = \exp\left(i \frac{u_y}{\hbar v_F q} \sin qx \right). \tag{6}$$

It is easy to verify that

$$\begin{aligned} \tilde{H} = GHG^{-1} &= H - u_y \sigma^y \cos qx \\ &= H_0 + (u_x \sigma^x + u_z \sigma^z) \cos qx. \end{aligned} \tag{7}$$

With u_y eliminated, we can construct the mirror transformation

$$\mathcal{P}_x = \Pi_y K. \tag{8}$$

The only term that can possibly be affected by this compounded transformation is actually invariant,

$$\begin{aligned} &\Pi_y K[\tfrac{\hbar v_F}{i}(-\sigma^x \partial_y)] K^{-1} \Pi_y \\ &= \Pi_y [\tfrac{\hbar v_F}{i}(\sigma^x \partial_y)] \Pi_y = \tfrac{\hbar v_F}{i}(-\sigma^x \partial_y), \end{aligned} \tag{9}$$

so that $\mathcal{P}_x \tilde{H} \mathcal{P}_x^{-1} = \tilde{H}$. Since complex conjugation imposes $(k_x, k_y) \to (-k_x, -k_y)$, and Π_y reverses $-k_y$ back to k_y, we have:

$$|-k_x, k_y; \alpha\rangle = \mathcal{P}_x \, |k_x, k_y; \alpha\rangle \, , E_{-k_x,k_y;\alpha} = E_{k_x,k_y;\alpha}. \tag{10}$$

By compounding $\mathcal{P}_x$ with time reversal, $\tilde{\mathcal{T}}$, we also obtain a reflection about the x-axis: $\tilde{\mathcal{T}}\mathcal{P}_x : (k_x, k_y) \to (k_x, -k_y)$. Below we will first discuss the equations describing the photocurrent response of the device, and then consider the consequences of the symmetries on the resulting photocurrent.

Within Fermi's golden rule, we expect that the photocurrent response to a particular frequency will be quadratic in the photon field. We restrict ourselves to normally incident photons, at frequencies which allow us to approximate the vector potential as spatially uniform, $\mathbf{A}(\mathbf{x}, t) = \mathrm{Re}\mathbf{A}_0(\omega) e^{i\omega t}$. Then, the $k, m, n = x, y$ component of the photocurrent is quite generally given by:

$$j_k(\omega) = \frac{e\tau}{4\hbar} \left(\frac{v_F^2}{\omega^2} \right) E_m(\omega) \mathcal{Q}_{kmn}(\omega) E_n^*(\omega). \tag{11}$$

Here, repeated indices are summed, $\mathbf{E}(\omega) = -i\omega \mathbf{A_0}$, and the factor $1/4$ appears since at zero temperature, only the $e^{-i\omega t}$ part contributes to the optical transitions. Also, in Eq. (39) we assume that the current decays on a time scale τ. Quite remarkably, in the presence of a periodic structure of magnetic strips lying along the y-axis, we will find that there is only one independent element of $\mathcal{Q}_{kmn}(\omega)$ which is nonzero:

$$\mathcal{Q}(\omega)_{y,x,y} = \mathcal{Q}(\omega)^*_{y,y,x} = -\mathcal{Q}(\omega)_{y,y,x}.$$

To calculate $\mathcal{Q}_{kmn}(\omega)$, we first write the surface photon-electron interaction, which we assume follows the minimal coupling prescription:

$$\hat{H}_{int} = e \frac{\partial H_0}{\partial \mathbf{p}} \cdot \mathbf{A}(\mathbf{x}, t). \tag{12}$$

The photon field can excite electrons from any subband of the valence band to any subband of the conduction band, and at any momentum. Therefore:

$$\mathcal{Q}_{kmn}(\omega) = \int \frac{d^2k}{(2\pi)^2} \sum_{\alpha>0, \beta<0} \mathcal{Q}^{\alpha\beta}_{kmn}(\mathbf{k}, \omega), \tag{13}$$

where $\mathcal{Q}^{\alpha\beta}_{kmn}(\mathbf{k}, \omega)$ accounts for excitations from the valence band $\beta < 0$ to the conduction band $\alpha > 0$ at momentum $\mathbf{k}$. Fermi's golden rule yields:

$$\begin{aligned} \mathcal{Q}^{\alpha\beta}_{kmn}(\mathbf{k}, \omega) = \hat{\mathbf{x}}_k \cdot \left(\mathbf{v}^{(\alpha)}_{\mathbf{k}} - \mathbf{v}^{(\beta)}_{\mathbf{k}} \right) M^{\alpha\beta}_{mn}(\mathbf{k}) \\ \times 2\pi \delta(\mathrm{E}^{(\alpha)}_{\mathbf{k}} - \mathrm{E}^{(\beta)}_{\mathbf{k}} - \omega), \end{aligned} \tag{14}$$

where the velocities in the band α are given by $\mathbf{v}_{\mathbf{k}}^{(\alpha)} = \langle \mathbf{k};\alpha| \frac{\partial H_0}{\partial \mathbf{p}} |\mathbf{k};\alpha\rangle$, and the matrix elements are given by

$$M_{mn}^{\alpha\beta}(\mathbf{k}) = \langle \mathbf{k},\alpha| \Gamma_m |\mathbf{k},\beta\rangle \langle \mathbf{k},\beta| \Gamma_n^\dagger |\mathbf{k},\alpha\rangle , \tag{15}$$

with $\Gamma_m = e\frac{\partial H_0}{\partial \mathbf{p}} \cdot \hat{\mathbf{x}}_m$. From this definition it is clear that $M_{mn}^{\alpha\beta}(\mathbf{k}) = \left(M_{nm}^{\alpha\beta}(\mathbf{k})\right)^*$, i.e., it is hermitian.

The calculation of the photocurrent response in the presence of the magnetic texture can now follow. We first define

$$\widetilde{\mathcal{Q}}_{kmn}^{\alpha\beta}(\mathbf{k}) = \sum_{\sigma,\sigma'=\pm 1} \mathcal{Q}_{kmn}^{\alpha\beta}(\sigma k_x, \sigma' k_y), \tag{16}$$

which sums the contributions of the four mirror-related momenta, $(\pm k_x, \pm k_y)$, and is defined for $k_x, k_y > 0$. This definition takes into account all symmetry-related current cancellations. Assuming that u_y has been gauged away, we use Eqs. (4) and (10) to connect the contributions arising from the four momenta $(\pm k_x, \pm k_y)$. Due to these symmetries, along with the particle-hole transformation, Eq. (5), we have:

$$\begin{gathered} v_x^\alpha(\sigma k_x, \sigma' k_y) = \sigma v_x^\alpha(k_x, k_y), \\ v_y^\alpha(\sigma k_x, \sigma' k_y) = \sigma' v_y^\alpha(k_x, k_y), \\ \mathbf{v}^\alpha(\mathbf{k}) = -\mathbf{v}^{-\alpha}(\mathbf{k}) \end{gathered} \tag{17}$$

for $\sigma, \sigma' = \pm 1$.

The same symmetries, applied to the matrix elements yield the relations

$$\begin{aligned} \tilde{\mathcal{T}}: \quad M_{mn}^{\alpha\beta}(-\mathbf{k}) &= M_{nm}^{\alpha\beta}(\mathbf{k}) \\ \mathcal{P}_x: \quad M_{xy}^{\alpha\beta}(-k_x, k_y) &= -M_{yx}^{\alpha\beta}(\mathbf{k}) \\ \mathcal{P}_x: \quad M_{nn}^{\alpha\beta}(-k_x, k_y) &= M_{nn}^{\alpha\beta}(\mathbf{k}). \end{aligned} \tag{18}$$

The diagonal elements, $M_{nn}^{\alpha\beta}(\mathbf{k})$, are the same at all four points $(\pm k_x, \pm k_y)$. This makes their contribution to a current in any direction cancel identically, since the velocities obey the mirror symmetries in Eq. (17). From Eqs. (17) and (18), we find that the only nonzero elements of the tensor $\widetilde{\mathcal{Q}}_{kmn}^{\alpha\beta}(\mathbf{k})$ are

$$\widetilde{\mathcal{Q}}_{yxy}^{\alpha\beta}(\mathbf{k}) = 4i \left[(v_y^{|\alpha|}(\mathbf{k}) + v_y^{|\beta|}(\mathbf{k}) \right] \mathrm{Im}\left[M_{xy}^{\alpha\beta}(\mathbf{k})\right] \tag{19}$$

and $\widetilde{\mathcal{Q}}_{yyx}^{\alpha\beta}(\mathbf{k}) = -\widetilde{\mathcal{Q}}_{yxy}^{\alpha\beta}(\mathbf{k})$. These conclusions confirm our claim regarding the photo-response tensor, $\mathcal{Q}_{kmn}(\omega)$ defined in Eq. (34): It has only one independent nonzero contribution, $\mathcal{Q}_{yxy}(\omega) = -\mathcal{Q}_{yyx}(\omega)$, which is imaginary. This implies that the current in the x direction vanishes, i.e., the photocurrent is always parallel to the magnetic pattern. Furthermore, this current is only induced by the circular component of the incident light.

This result also lets us determine what magnetic patterning vector $\mathbf{u}$ is necessary for a finite response. As it turns out, having either $u_x = 0$ or $u_z = 0$ leads to $\mathrm{Im}M_{xy}^{\alpha\beta} = 0$, and to a vanishing response. To see this, consider the composite transformation $U = \Pi_x \Pi_y \sigma^z \tilde{\mathcal{T}}$. The first part of the transformation, $\Pi_x \Pi_y \sigma^z$, implements a π rotation on the bare model, H_0, and leaves it invariant. If $u_x = u_y = 0$, then $H^{(z)} = H_0 + u_z \sigma^z \cos(qx)$ is also invariant this transformation. $\tilde{\mathcal{T}}$ then leaves $H^{(z)}$ invariant, and reverses momentum directions. Together, they make an anti-unitary transformation which leaves the momentum $\mathbf{p}$ invariant. Its effect on the transition matrix is $M_{mn}^{\alpha\beta}(\mathbf{k}) = M_{nm}^{\alpha\beta}(\mathbf{k}) = M_{mn}^{\alpha\beta}(\mathbf{k})^*$. The same relation is obtained also for the case $u_z = 0$ with a finite u_x, with UM used instead of U (with M the half-period translation operator). Thus both u_z and u_x must be finite for a finite photo-response.

The summed momentum-specific photocurrent contributions, $\widetilde{\mathcal{Q}}_{kmn}^{\alpha\beta}(\mathbf{k})$, can be found analytically to lowest order in the strength of the magnetic texture. To do so, we expand the eigenstates of the Hamiltonian that appear in the definition of $M_{mn}^{\alpha\beta}(\mathbf{k})$ in Eq. (15), and also separate the current inducing processes $\widetilde{\mathcal{Q}}_{kmn}^{\alpha\beta}(\mathbf{k})$ according to channels of interband scattering. In terms of momenta in the *extended* BZ, the possible scattering processes to order V^2 are $\mathbf{k} \to \mathbf{k} + q$, $\mathbf{k} \to \mathbf{k} - q$, and $\mathbf{k} \to \mathbf{k}$. The resulting photocurrent can be written as

$$\widetilde{\mathcal{Q}}_{yxy}^{\mathrm{ext}}(\mathbf{k}) = 2\pi u_x u_z (e v_F)^2 \sum_{\lambda=0,+,-} F_\lambda(\mathbf{k}) \delta_\lambda(\omega, \mathbf{k}), \tag{20}$$

where the functions F_λ, $\lambda = +, -, 0$ account for the above scattering processes and are given by

$$\begin{aligned} F_0(\mathbf{k}) &= v_F \frac{-512 i k_y^2 k_x^2}{|\mathbf{k}|^2(-4k_x^2 + \mathbf{q}^2)^2} \\ F_\pm(\mathbf{k}) &= v_F \frac{8 i k_y^2 q^2}{|\mathbf{k}|^2 \, |\mathbf{k} \pm \mathbf{q}|^2 (|\mathbf{k} \pm \mathbf{q}|^2 - |\mathbf{k}|^2)^2}. \end{aligned} \tag{21}$$

The delta functions in Eq. (54) were abbreviated to $\delta_\lambda(\omega, \mathbf{k}) = \delta(E_{\mathbf{k}+\lambda\mathbf{q}} + E_{\mathbf{k}} - \omega)$. The momentum integrated response tensor becomes $\mathcal{Q}_{kmn}(\omega) = \int \frac{d^2k}{2\pi} \widetilde{\mathcal{Q}}_{kmn}^{\mathrm{ext}}(\mathbf{k})$, where the integral is taken over the $k_x, k_y > 0$ quadrant of the *extended* BZ [24] (see supplemental material for more information).

Our results are best expressed in terms of the intensity, I, of the light field. For a coherent monochromatic circularly polarized wave with electric-field amplitude E_0, we have $I = \epsilon_0 c E_0^2$. This yields the current response:

$$j_y(\omega) = \frac{e^3 v_F^2 q \tau}{\epsilon_0 c \hbar^2} \frac{I}{\omega^2} \eta(\omega) \tag{22}$$

in terms of the dimensionless frequency-dependent response, $\eta(\omega)$, defined by $\mathcal{Q}_{yxy}(\omega) = 2\frac{e^2 v_F^2 q}{\hbar} \eta(\omega)$. For a continuous spectrum with intensity per unit angular frequency, containing both circular polarizations, we write $I(\omega)d\omega = 2\epsilon_0 c |\mathbf{E}(\omega)|^2$. The total current response is then:

$$j_y = \frac{e^3 v_F^2 q \tau}{2\epsilon_0 c \hbar^2} \int_0^\Omega \frac{I(\omega)}{\omega^2} \eta(\omega) d\omega, \tag{23}$$

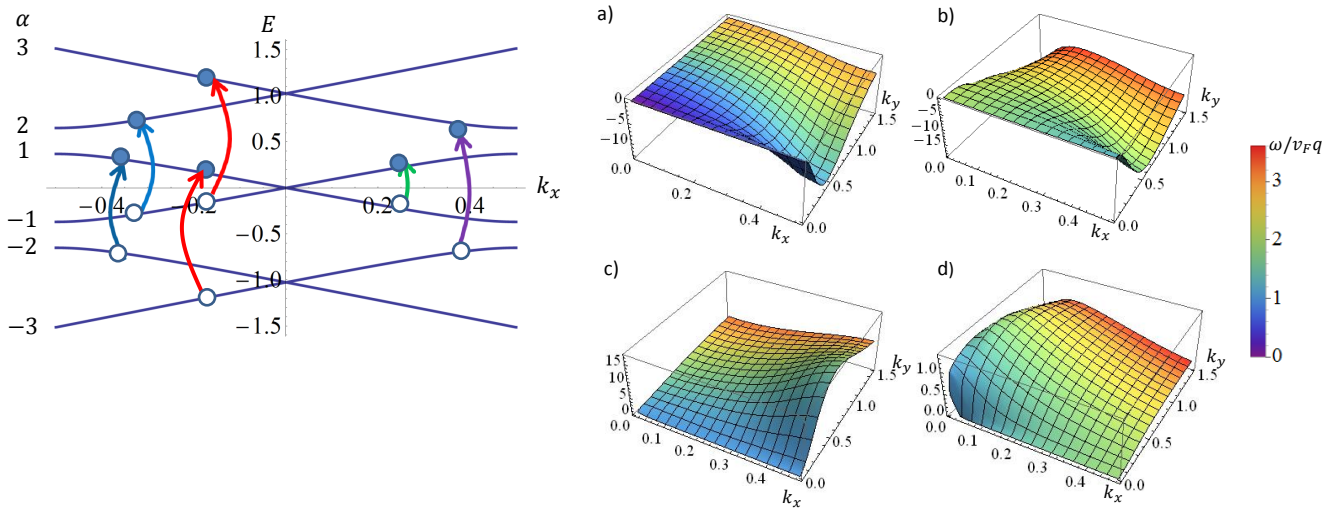

Figure 2: Top left: Effective bandstructure of the proposed heterostructure, cut along the line $k_y = 0$ (units such that $|\mathbf{q}| = 1$). Band indices are shown on the left. Transitions contributing to the summed momentum specific tensor $\mathcal{Q}^{\alpha\beta}_{kmn}(\mathbf{k})$ are depicted by arrows. (a)-(d) Numerical results for $\int d\omega \tilde{\mathcal{Q}}^{\alpha\beta}_{yxy}(\mathbf{k})$, in units of $\frac{e^2 v_F^3}{c^2}$. The colors indicate the photon frequency of the transition as determined by the δ functions in Eq. (54). Panels (a) and (b) contain the tensors for the transitions $(\alpha, \beta) = (1, -1)$ and $(2, -2)$, respectively, in which the excitation leaves the electron momentum unchanged. These transitions indicated by green and blue arrows in the top left panel renormalize the conduction and valence bands. (c) Same for $(\alpha, \beta) = (2, -1)$ and $(1, -2)$ (purple arrows in the top left panel). (d) Same for $(\alpha, \beta) = (3, -1)$ and $(1, -3)$ (red arrows).

.

where Ω is the high-frequency cutoff.

Fig. 3 displays our numerical results for the dimensionless response $\eta(\omega)$ for three magnetic patterning strengths. We make three observations: (1) Most of the contribution to the current density arises from frequencies $\omega > v_F q$. (2) For $\omega \gg v_F q$, the dimensionless response $\eta(\omega)$ approaches a constant. (3) $\eta(\omega)$ changes sign at $\Omega^* \sim v_F q$. The latter observation can also be deduced from Eq. (21), as $F_0(\mathbf{k})$ differs in sign from the two other contributions, and dominates below Ω^*.

In order to get some intuition for the origin of the photocurrent contributions, we study the momentum-specific response $\tilde{\mathcal{Q}}^{\alpha\beta}_{yxy}(\mathbf{k}, \omega)$. This quantity allows us to understand which parts of the BZ contribute most to the effect. This function is plotted in Figs 2 (a-d), where in addition to the response as a function of momentum, the photon energy responsible for the transition at each momentum is encoded in the color. We see that the effect is not exclusively due to the edges of the BZ. Rather, the contribution is uniformly distributed in momentum space, validating a perturbative perspective on the effects of the magnetic surface texture.

A particularly appealing application of the magnetically patterned surface is solar energy harvesting, particularly in the IR range. The intensity spectrum of the sun, for low frequencies, is approximately given by the Rayleigh-Jeans law, $I = \frac{k_B T_{sun}}{4\pi^2 c^2}\omega^2$. At the Earth's distance from the sun, at normal incidence we expect this to be suppressed by $(R_{sun}/R_{Sun-Earth})^2 \approx 0.5 \cdot 10^{-4}$. Combined, this yields the 2d closed-circuit current expected for normally incident sunlight:

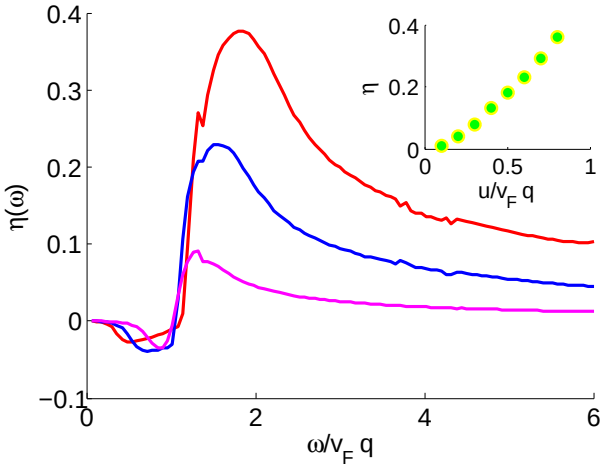

Figure 3: The dimensionless response function $\eta(\omega)$, for $u_x/\hbar v_F q = u_z/\hbar v_F q = 0.1, 0.2, 0.3$ $u_x = u_z = 0.2\hbar v_F q$ (purple, blue and red, respectively). The horizontal axis gives the frequency ω in units of $v_F q$. The inset shows the saturation value η of the response function at high frequencies $\omega \gg v_F q$, as a function of $u/\hbar v_F q$, with $u = u_x = u_z$.

$$j_y^{(solar)} \approx \frac{e^3 v_F^2 q \tau}{2\epsilon_0 c \hbar^2} \frac{k_B T_{sun}}{4\pi^2 c^2} \left(\frac{R_{sun}}{R_{Sun-Earth}}\right)^2 E_{gap} \eta, \quad (24)$$

where E_{gap} is the bandgap of the topological insulator

hosting the Dirac cone, and η is the constant characterizing $\eta(\omega)$ at frequencies $\omega \gg v_F q$. For low magnetic coupling, we obtain $\eta \approx 2(\frac{u}{\hbar v_F q})^2$, as can be seen from Fig. 3. For a typical Fermi velocity of $v_F = 5 \cdot 10^5 \frac{m}{sec}$ we have that $\eta = 0.1$ corresponds to a reasonable magnetic coupling of about $7.2meV$. Further taking a typical bandgap of $E_{gap} \approx 0.3eV$, the wavenumber of the magnetic structure $q = 10^8 m^{-1}$, and a scattering time of $\tau = 1ps$, we have $j \approx 5\eta \times 10^{-7} \frac{A}{m}$.

The effect can also easily be explored using monochromatic laser light. Using the same parameters as above, Eq. (22) yields:

$$j_y \approx 2 \cdot 10^{21} \frac{I}{\omega^2} \tilde{\eta}(\omega) \ \ \frac{Am}{Jsec} \tag{25}$$

For laser light of intensity $I = 10^5 W/m^2$ at angular frequency $\omega = 3 \cdot 10^{14} s^{-1}$, with $\eta(\omega) \sim 1$ this yields $j_y \sim 2 \cdot 10^{-3} A/m$.

The unique properties of the surfaces of topological insulators beg to be translated into practical applications. The lack of a generic photocurrent response on such surfaces so far has stifled the possibility of applications in light detection and photovoltaics. In this manuscript we demonstrated how surface magnetic patterning employs the spin-orbit locking, and allows for a substantial photocurrent response even to low-intensity sources such as the low-energy solar spectrum. The surface is naturally sensitive to photon energies below $0.3eV$, as opposed to semiconductor based photovoltaics, which require energies that exceed the material's bandgap. As such, this effect can be used for detection of micrometer wavelength radiation - a range with limited detection schemes.

Many aspects remain unexplored. To understand how the TI surface could be harnessed for solar energy harvesting, we need to understand what the natural open-circuit voltage is. In addition, we have only provided a crude account of disorder effects on the surface, and completely ignored the possibility of bulk contributions at high frequencies. Lastly, we are confident that the magnitude of the effect could be improved by optimizing our device by using other magnetic patterns, or different materials. For instance, we expect that a similar effect will exist in arrays of 2d topological insulator strips, e.g., HgTe/CdTe heterostructures, put in an in-plane spatially varying field. We intend to explore at least some of these issues in future work.

We acknowledge financial support from the Packard Foundation, the IQIM - an NSF center funded in part by the Gordon and Betty Moore Foundation - and especially DARPA through FENA (Caltech), through SPP 1666 of the Deutsche Forschungsgemeinschaft and the Helmholtz Virtual Institute "New States of Matter and Their Excitations" (Berlin), as well as the Bi-National Science Foundation and I-Core: the Israeli Excellence Center "Circle of Light" (Haifa).

[1] D. Muhlbacher, M. Scharber, M. Morana, Z. Zhu, D. Waller, R. Gaudiana, and C. Brabec, Advanced Materials **18**, 2884 (2006).
[2] B. Evaand and F. C. Krebs, Solar Energy Materials and Solar Cells **91**, 954 (2007).
[3] S. H. Park, A. Roy, S. Beaupre, S. Cho, N. Coates, J. S. Moon, D. Moses, M. Leclerc, K. Lee, and A. J. Heeger, Nature Photonics **3**, 297 (2009).
[4] R. R. Lunt and V. Bulovic, Applied Physics Letters **98**, 113305 (2011).
[5] H. Ago, K. Petritsch, M. S. P. Shaffer, A. H. Windle, and R. H. Friend, Advanced Materials **11**, 1281 (1999).
[6] E. Kymakis and G. A. J. Amaratunga, Applied Physics Letters **80**, 112 (2002).
[7] R. M. Jain, R. Howden, K. Tvrdy, S. Shimizu, A. J. Hilmer, T. P. McNicholas, K. K. Gleason, and M. S. Strano, Advanced Materials **24**, 4436 (2012).
[8] H. A. Atwater and A. Polman, Nature Materials **9**, 205 (2010).
[9] M. T. Sheldon and H. A. Atwater, `arXiv:1202.0301` .
[10] K. Nakayama, K. Tanabe, and H. A. Atwater, Applied Physics Letters **93**, 121904 (2008).
[11] L. Fu, C. L. Kane, and E. J. Mele, Phys. Rev. Lett. **98**, 106803 (2007).
[12] H. Zhang, C.-X. Liu, X.-L. Qi, X. Dai, Z. Fang, and S.-C. Zhang, Nat Phys **5**, 438 (2009).
[13] J. E. Moore and L. Balents, Phys. Rev. B **75**, 121306 (2007).
[14] D. Hsieh, D. Qian, L. Wray, Y. Xia, Y. S. Hor, R. J. Cava, and M. Z. Hasan, Nature **452**, 970 (2008).
[15] Y. Xia, D. Qian, D. Hsieh, L. Wray, A. Pal, H. Lin, A. Bansil, D. Grauer, Y. S. Hor, R. J. Cava, and M. Z. Hasan, Nat Phys **5**, 398 (2009).
[16] X.-L. Qi, T. L. Hughes, and S.-C. Zhang, Phys. Rev. B **78**, 195424 (2008).
[17] X.-L. Qi, R. Li, J. Zang, and S.-C. Zhang, Science **323**, 1184 (2009).
[18] A. M. Essin, J. E. Moore, and D. Vanderbilt, Physical Review Letters **102**, 146805 (2009).
[19] P. Hosur, Phys. Rev. B **83**, 035309 (2011).
[20] A. Junck, G. Refael, and F. von Oppen, Phys. Rev. B **88**, 075144 (2013).
[21] N. M. Gabor, J. C. W. Song, Q. Ma, N. L. Nair, T. Taychatanapat, K. Watanabe, T. Taniguchi, L. S. Levitov, and P. Jarillo-Herrero, Science **334**, 648 (2011).
[22] J.W. McIver, D. Hsieh, H. Steinberg, P. Jarillo-Herrero, and N. Gedik, Nat. Nanotech. **7**, 96 (2011).
[23] L. Fu, Phys. Rev. Lett. **103**, 266801 (2009).
[24] The mapping between the band index α and momentum $\mathbf{k}$ in the reduced BZ, and the extended zone momenta is given by $\mathbf{k}; \alpha \to \mathbf{k} - (-1)^{\alpha} \lfloor \frac{\alpha}{2} \rfloor \mathbf{q}$. Note that the divergences cancel between $F_0(\mathbf{k})$ and $F_{\pm}(\mathbf{k})$

SUPPLEMENTARY MATERIALS

PHOTOCURRENT DUE TO THE SOLAR SPECTRUM

We begin with

$$j = e \int \frac{d^2k}{(2\pi)^2} \sum_{\alpha} \left[\mathbf{v}_{\alpha,\mathbf{k}} (n_{\mathbf{k},\alpha} - n^0_{\mathbf{k},\alpha}) \right] \tag{26}$$

where $n^0_{\mathbf{k},\alpha}$is the equilibrium distribution function, and $n_{\mathbf{k},\alpha}$is the distribution function induced by the incident light. Assuming the chemical potential is at the Dirac point, within the relaxation time approximation we write,

$$(n_{\mathbf{k},\alpha} - n^0_{\mathbf{k},\alpha}) = \tau \sum_{\beta<0} \Gamma(\mathbf{k}, \beta \to \mathbf{k}, \alpha)(n^0_{\mathbf{k},\beta} - n^0_{\mathbf{k},\alpha}), \qquad \alpha > 0$$

and

$$(n_{\mathbf{k},-\beta} - n^0_{\mathbf{k},-\beta}) = -(n_{\mathbf{k},\beta} - n^0_{\mathbf{k},\beta}), \qquad \beta > 0.$$

For $T = 0$, we have

$$j = e\tau \int \frac{d^2k}{(2\pi)^2} \sum_{\alpha>0,\beta<0} \left[\mathbf{v}_{\alpha,\mathbf{k}} \Gamma(\mathbf{k}, \beta \to \mathbf{k}, \alpha) - \mathbf{v}_{\beta,\mathbf{k}} \Gamma(\mathbf{k}, \beta \to \mathbf{k}, \alpha) \right]. \tag{27}$$

The transition rates are given by Fermi's golden rule

$$\Gamma(\mathbf{k}, \beta \to \mathbf{k}, \alpha) = \frac{|\langle \mathbf{k}, \alpha | H_{int}(\omega) | \mathbf{k}, \beta \rangle|^2}{\hbar} 2\pi\delta(E_{\mathbf{k},\alpha} - E_{\mathbf{k},\beta} - \omega) \tag{28}$$

for a time dependent Hamiltonian containing a single frequency.

The interaction hamiltonian is written as

$$\hat{H}_{int} = e \frac{\partial H_0}{\partial \mathbf{p}} \cdot \mathbf{A}(\mathbf{x}, t) \tag{29}$$

We assume a circularly polarized light:

$$\mathbf{E}(t) = E_c(\hat{x} \cos\omega t + \hat{y} \sin\omega t) \tag{30}$$

This corresponds to a vector potential

$$\begin{array}{c} \mathbf{A}(\omega) = \frac{E_c}{\omega}(\hat{x} \sin\omega t - \hat{y} \cos\omega t) \\ = \frac{1}{2i}\frac{E_c}{\omega}((\hat{x} - i\hat{y})e^{i\omega t} - (\hat{x} + i\hat{y})e^{-i\omega t}), \end{array} \tag{31}$$

,

The current response to this field is:

$$j_k = \frac{e\tau}{\hbar} (ev_F)^2 \left(\frac{1}{\omega^2} \right) E_m(\omega) \mathcal{Q}_{kmn}(\omega) E^*_n(\omega). \tag{32}$$

where $E_x(\pm\omega) = E_c/2$, $E_y(\omega) = \pm\frac{E_c}{2i}$.

The $\mathcal{Q}_{kmn}(\omega)$ tensor, is given by integrating over the momentum resolved $\mathcal{Q}^{\alpha\beta}_{kmn}(\mathbf{k}, \omega)$ as

$$\mathcal{Q}_{kmn}(\omega) = \int \frac{dk_x dk_y}{(2\pi)^2} \sum_{\alpha>0,\beta<0} \mathcal{Q}^{\alpha\beta}_{kmn}(\mathbf{k}, \omega). \tag{33}$$

The momentum resolved $\mathcal{Q}^{\alpha\beta}_{kmn}(\mathbf{k},\omega)$ are in turn given by

$$\begin{aligned}\mathcal{Q}^{\alpha\beta}_{kmn}(\mathbf{k},\omega) &= \hat{\mathbf{x}_k}\cdot\left(\mathbf{v}^{(\alpha)}_{\mathbf{k}} - \mathbf{v}_{\mathbf{k}}{}^{(\beta)}\right) M^{\alpha\beta}_{mn}(\mathbf{k}) \\ &\quad\times 2\pi\delta(\mathrm{E}^{(\alpha)}_{\mathbf{k}} - \mathrm{E}^{(\beta)}_{\mathbf{k}} - \hbar\omega),\end{aligned} \tag{34}$$

The matrix elements are *dimensionless*, and given by:

$$M^{\alpha\beta}_{mn}(\mathbf{k}) = \langle\mathbf{k},\alpha|\sigma_m|\mathbf{k},\beta\rangle\langle\mathbf{k},\beta|\sigma^\dagger_n|\mathbf{k},\alpha\rangle. \tag{35}$$

In the following, we carry out the calculation for a non-monochromatic source of light, which has an intensity ditribution as a function of angular frequency, $I(\omega)$. The monochromatic limit is easy to extract, by setting $I(\omega)$ to be proportional to a delta-function. The intensity of light at a given frequency with amplitude E_x and E_y is:

$$I(\omega)d\omega = \frac{1}{2}\epsilon_0 c(E_x^2 + E_y^2) \tag{36}$$

The $1/2$ comes from averaging the $\cos^2(\omega t)$, $\sin^2(\omega t)$ over time. For the two circular polarizations of light this gives:

$$I(\omega)d\omega = \frac{1}{2}\epsilon_0 c(2E_{c+}^2 + 2E_{c-}^2) = \epsilon_0 c(E_{c+}^2 + E_{c-}^2) = 2\epsilon_0 c E_{c+}^2 \tag{37}$$

where we assumed that the two circular polarizations have the same amplitude. So our circular polarization in terms of the solar intensity is:

$$E_c^2 = \frac{1}{2\epsilon_0 c} I(\omega)d\omega. \tag{38}$$

Collecting all the coefficients, and using the property of the tensor $\mathcal{Q}_{kmn}$, we get

$$j_y = \frac{e^3\tau v_F^2}{2\hbar c\epsilon_0}\int d\omega 2\mathcal{Q}_{yxy}(\omega)\frac{1}{4}\frac{I(\omega)}{\omega^2}. \tag{39}$$

We now define $\eta(\omega)$ as a dimensionless quantity that encodes the photocurrent respnse as a function of frequency, which also contains all the intrinsic numerical factors:

$$\eta(\omega) = \frac{1}{2(2\pi)^2}\int_{-q/2}^{q/2}\frac{dk_x}{2\pi q}\int_{-\infty}^{\infty}\frac{d\tilde{k}_y}{2\pi q}\hbar v_F q\frac{\mathcal{Q}_{yxy}(\mathbf{k},\,\omega)}{v_F}, \tag{40}$$

Using this quantity in Eq. (39) , we get:

$$j_y = \frac{e^3\tau v_F^2 q}{2c\epsilon_0\hbar^2}\int d\omega\eta(\omega)\frac{I(\omega)}{\omega^2} \tag{41}$$

Now let us substitute $I(\omega)$ for the sun. For a blackbody at Temperature T, the black body luminosity per ω is:

$$I(\omega,T) = \frac{1}{4\pi^2}\frac{\hbar\omega^3}{c^2}\frac{1}{\exp(\hbar\omega/k_BT)-1} \tag{42}$$

where $I(\nu,T)$ is the energy per unit time (or the power) radiated per unit area of emitting surface in the normal direction per unit solid angle per unit frequency by a black body at temperature T. The power per unit area arriving at the earth, and assuming normal incidence is:

$$I_{SE}(\omega,T_{sun}) = \frac{R_{sun}^2}{R_{earth}^2}I(\omega,T_{sun}) \tag{43}$$

For low frequencies, we can approximate the black body spectrum as

$$I(\omega,T) = \frac{k_BT\omega^2}{4\pi^2c^2} \tag{44}$$

which is the Rayleigh-Jeans law. Inserting this into Eq.41, and taking $\eta(\omega) = \tilde{\eta}$ (appropriate for large frequencies) ,we get

$$j_y = \frac{e^3 \tau v_F^3 q^2}{2c\epsilon_0 \hbar^2} \tilde{\eta} \mathcal{I}_0 \frac{\omega_{max}}{v_F q} \tag{45}$$

where the constant

$$\mathcal{I}_0 = \frac{k_B T_{sun}}{c^2 (2\pi)^2} \left(\frac{R_{sun}^2}{R_{earth}^2} \right) \tag{46}$$

Furthermore, taking

$$\omega_{max} = \frac{E_{gap}}{\hbar} \tag{47}$$

we get

$$j_y = \frac{e^3 \tau v_F^2 q}{2c\epsilon_0 \hbar^3} \tilde{\eta} \mathcal{I}_0 E_{gap}. \tag{48}$$

Altogether, this is: with $\tilde{\eta} \approx 0.2$ for $|u| = 0.5$, and $E_{gap} = 0.3ev$, $v_F = 5 \cdot 10^5 m$, $\tau = 10^{-12} sec$ and $q = \times 10^8 m^{-1}$, we get

$$j = 3 \cdot 10^{-7} \frac{A}{m} = 3 \cdot 10^{-9} \frac{A}{cm}. \tag{49}$$

This can yield, in a device containing strips of width $30nm$ of magnetically coupled topological insulators,

$$j = \cdot 10^{-3} \frac{A}{cm^2}. \tag{50}$$

PERTURBATIVE ANALYSIS OF THE PHOTOCURRENT RESPONSE

In the following, we shall calculate the response tensor, accounting for the surface magnetic pattern within second order perturbation theory. This can be most conveniently expressed using momenta in the extended Brillouin zone. Denoting by $|\psi^{(0)}(\mathbf{k}, \alpha)\rangle$ the eigenstates of H_0 (without the magnetic structure), we expand the eigenstates in second order perturbation theory in $V = V^+ + V^- = (\mathbf{u} \cdot \vec{\sigma}) e^{i\mathbf{q}\cdot r} + h.c.$, as

$$|\psi(\mathbf{k}, \alpha)\rangle = |\psi^{(0)}(\mathbf{k}, \alpha)\rangle + |\psi^{(1)}(\mathbf{k}, \alpha)\rangle + |\psi^{(2)}(\mathbf{k}, \alpha)\rangle \tag{51}$$

with $\alpha = c, v$ for conduction and valence bands. The first and second order corrections are given by

$$|\psi^{(1)}(\mathbf{k}, \alpha)\rangle = \sum_{\sigma=\pm} \frac{1}{E_{\mathbf{k}}^{\alpha} - H(\mathbf{k} + \sigma\mathbf{q})} V^{\sigma} |\psi^{(0)}(\mathbf{k}, \alpha)\rangle \tag{52}$$

and

$$\begin{aligned} |\psi^{(2)}(\mathbf{k}, v)\rangle &= P_{\mathbf{k}}^c \sum_{\sigma=\pm} \frac{1}{E_{\mathbf{k}}^v - E_{\mathbf{k}}^c} V^{\sigma\dagger} \frac{1}{E_{\mathbf{k}}^v - H(\mathbf{k} + \sigma\mathbf{q})} V^{\sigma} |\psi^{(0)}(\mathbf{k}, v)\rangle. \\ |\psi^{(2)}(\mathbf{k}, c)\rangle &= P_{\mathbf{k}}^v \sum_{\sigma=\pm} \frac{1}{E_{\mathbf{k}}^c - E_{\mathbf{k}}^v} V^{\sigma\dagger} \frac{1}{E_{\mathbf{k}}^c - H(\mathbf{k} + \sigma\mathbf{q})} V^{\sigma} |\psi^{(0)}(\mathbf{k}, c)\rangle. \end{aligned} \tag{53}$$

where $P_{\mathbf{k}}^c$ is a projector on the conduction band state with momentum $\mathbf{k}$. In second order perturbation theory, the total photocurrent response can be written as

$$\mathcal{Q}_{yxy}^{\text{ext}}(\mathbf{k}) = 2\pi (e v_F)^2 \sum_{\lambda=0,+,-} \hat{\mathbf{y}} \cdot \left(v_{\mathbf{k}+\lambda\mathbf{q}}^c - v_{\mathbf{k}}^v \right) M_{xy}^{\lambda}(\mathbf{k}) \delta_{\lambda}(\omega, \mathbf{k}) \tag{54}$$

where $v^v_{\mathbf{k}}$ and $v^c_{\mathbf{k}}$ denote the velocities in the conduction and valence bands, and the delta functions in Eq. (54) were abbreviated to $\delta_\lambda(\omega,\mathbf{k}) = \delta(E^c_{\mathbf{k}+\lambda\mathbf{q}} + E^v_{\mathbf{k}} - \omega)$. The index $\lambda = 0, +1, -1$ denotes process which correspond to $\mathbf{k}, v \to \mathbf{k}, c$, $\mathbf{k}, v \to \mathbf{k}+\mathbf{q}, c$ and $\mathbf{k}, v \to \mathbf{k}-\mathbf{q}, c$, respectively. Our goal is to calculate the matrix elements:

$$M^\lambda_{mn}(\mathbf{k}) = \langle\psi(\mathbf{k}+\lambda\mathbf{q},c)|\,\sigma_m|\psi(\mathbf{k},v)\rangle\,\langle\psi(\mathbf{k},v)|\,\sigma_n|\psi(\mathbf{k}+\lambda\mathbf{q},c)\rangle, \tag{55}$$

to second order in V. First, we describe transitions from $\mathbf{k}, v \to \mathbf{k}+\mathbf{q}, c$ in the extended BZ. Two substitutions of $|\psi^{(1)}(\mathbf{k},v)\rangle$ from Eq. (52) into Eq. (55) yield

$$M^+_{mn}(\mathbf{k}) = \sum_{r,s} u_r u^*_s \left[F^{v,v}_{mrsn}(\mathbf{k}) + F^{v,c}_{mrns}(\mathbf{k}) + F^{c,v}_{rmsn}(\mathbf{k}) + F^{c,c}_{rmns}(\mathbf{k})\right] \tag{56}$$

where

$$F^{\alpha\beta}_{mnrs}(\mathbf{k}) = \mathrm{Tr}\left[P^c_{\mathbf{k}+\mathbf{q}}\sigma_m R^\alpha_+(\mathbf{k})\sigma_n P^v_{\mathbf{k}}\sigma_r R^\beta_+(\mathbf{k})\sigma_s\right] \tag{57}$$

with $\alpha, \beta = v, c$ and

$$\begin{aligned} R^v_\pm(\mathbf{k}) &= \frac{1}{E^v_{\mathbf{k}} - H(\mathbf{k}\pm\mathbf{q})} \\ R^c_\pm(\mathbf{k}) &= \frac{1}{E^c_{\mathbf{k}\pm\mathbf{q}} - H(\mathbf{k})} \end{aligned} \tag{58}$$

Note the permutation of the indices in Eq. (59).

Next we compute the matrix elements for transitions which in the extended BZ, correspond to transitions $\mathbf{k} \to \mathbf{k}-\mathbf{q}$. By taking $\mathbf{q} \to -\mathbf{q}$ in Eq. (57,

$$M^-_{mn}(\mathbf{k}) = \sum_{r,s} u^*_r u_s \left[B^{v,v}_{mrsn}(\mathbf{k}) + B^{v,c}_{mrns}(\mathbf{k}) + B^{c,v}_{rmsn}(\mathbf{k}) + B^{c,c}_{rmns}(\mathbf{k})\right] \tag{59}$$

with

$$B^{\alpha\beta}_{mnrs}(\mathbf{k}) = \mathrm{Tr}\left[P^c_{\mathbf{k}-\mathbf{q}}\sigma_m R^\alpha_-(\mathbf{k})\sigma_n P^v_{\mathbf{k}}\sigma_r R^\beta_-(\mathbf{k})\sigma_s\right]. \tag{60}$$

Next, we calculate the elements M^0_{mn} which correspond to transitions $\mathbf{k}, v \to \mathbf{k}, c$. These can give a non zero contribution to the current in second order perturbation theory due to the renormalization of the bands, c.f. Eq. (53). This yields

$$\begin{aligned} M^0_{mn}(\mathbf{k}) \;=\; \sum_{r,s} u^*_r u_s \Big\{ & \frac{1}{E^v_{\mathbf{k}} - E^c_{\mathbf{k}}}\Big(W^+_{nmrs} + W^-_{nmsr} + W^+_{mnsr} + W^-_{mnrs}\Big) \\ & - \frac{1}{E^v_{\mathbf{k}} - E^c_{\mathbf{k}}}\Big(\tilde{W}^+_{mnrs} + \tilde{W}^-_{mnsr} + \tilde{W}^+_{nmsr} + \tilde{W}^-_{nmrs}\Big) \\ & + Z^+_{mnrs} + Z^-_{mnsr} + Z^+_{nmsr} + Z^-_{nmrs}\Big\}, \end{aligned} \tag{61}$$

where

$$\begin{aligned} W^\rho_{mnrs} &= \mathrm{Tr}\left[P^c_{\mathbf{k}}\sigma_m P^c_{\mathbf{k}}\sigma_n P^v_{\mathbf{k}}\sigma_r R^v_\rho(\mathbf{k})\sigma_s\right], \\ \tilde{W}^\rho_{mnrs} &= \mathrm{Tr}\left[P^v_{\mathbf{k}}\sigma_m P^v_{\mathbf{k}}\sigma_n P^c_{\mathbf{k}}\sigma_r \tilde{R}^c_\rho(\mathbf{k})\sigma_s\right], \\ Z^\rho_{mnrs} &= \mathrm{Tr}\left[P^c_{\mathbf{k}}\sigma_m P^v_{\mathbf{k}}\sigma_r R^v_\rho(\mathbf{k})\sigma_n \tilde{R}^c_\rho(\mathbf{k})\sigma_s\right], \end{aligned} \tag{62}$$

and where we have introduced the notation

$$\tilde{R}^c_\rho(\mathbf{k}) = \frac{1}{E^c_{\mathbf{k}} - H(\mathbf{k}\pm\mathbf{q})}. \tag{63}$$

In Eq. (61), the first (second) term arises due to the second order corrections to the valence (conduction) states at momentum $\mathbf{k}$, c.f. first (second) line in Eq. (53). The third term in Eq. (61) arises due to first order corrections (as in Eq. (52)) to both the valence and conduction bands.

To make a connection with the results presented in the main text, we would like to sum over momenta in the four quadrants of the BZ, and obtain the the momentum summed response tensor,

$$\widetilde{\mathcal{Q}}^{\rm ext}_{yxy}(\mathbf{k}) = \sum_{\sigma,\sigma'=\pm} \mathcal{Q}^{\rm ext}_{yxy}(\sigma k_x, \sigma' k_y) \tag{64}$$

Note that the energy differences obey the symmetries

$$E^c_{(k_x,k_y)+\lambda\mathbf{q}} - E^v_{(k_x,k_y)} = E^c_{(-k_x,k_y)-\lambda\mathbf{q}} - E^v_{(-k_x,k_y)}, \tag{65}$$

and the velocities obey the symmetries appearing in Eq. (17) of the main text. Using these symmetries, it is natural to define the functions $F_\lambda(\mathbf{k})$ which were used in Eq. (20) the main text,

$$F_\lambda(\mathbf{k}) = \sum_{\sigma,\sigma'=\pm} M^{\lambda\cdot\sigma}_{xy}(\sigma k_x, \sigma' k_y) \left(v^c_y(\mathbf{k}+\lambda\mathbf{q}) - v^v_y(\mathbf{k})\right) \sigma' \tag{66}$$

The functions $F_\lambda(\mathbf{k})$ sum the matrix elements for the four transitions $(k_x, \pm k_y) \to (k_x, \pm k_y) + \lambda\mathbf{q}$, and $(-k_x, \pm k_y) \to (-k_x, \pm k_y) - \lambda\mathbf{q}$. These transitions occur at the same photon frequency, by Eq. (65). Therefore, using the functions $F_\lambda(\mathbf{k})$, Eq. (54) can be written as

$$\widetilde{\mathcal{Q}}^{\rm ext}_{yxy}(\mathbf{k}) = 2\pi {\rm Re}\left\{u_x u_z^*\right\} (ev_F)^2 \sum_{\lambda=0,+,-} F_\lambda(\mathbf{k}) \delta_\lambda(\omega, \mathbf{k}) \tag{67}$$

Second order perturbation theory in the reduced Brillouin zone scheme

In this section, we will make the connetion between the response tensor $\widetilde{\mathcal{Q}}^{\rm ext}_{kmn}(\mathbf{k})$ obtained in second order perturbation theory, and the response tensor $\widetilde{\mathcal{Q}}^{\alpha\beta}_{kmn}(\mathbf{k})$ for the reduced Brillouin zone. First, we note the relation between the *unperturbed* eigenstates in the reduced BZ, which we denote by $|\mathbf{k}, \alpha\rangle$, with α a positive (negative) integer for bands with $E > 0$ ($E < 0$), to those in the extended BZ, which we denote by $|\psi^{(0)}(\mathbf{k}, a\rangle$, with $a = v, c$. We will be interested only in the quadrant with $k_x, k_y > 0$ due to the symmetries discussed in the main text.

$$|\mathbf{k}, \alpha\rangle \to \left|\psi^{(0)}\left(\mathbf{k} - (-1)^\alpha \lfloor \frac{\alpha}{2} \rfloor \mathbf{q}, a\right)\right\rangle, \tag{68}$$

where in the above equation, set $a = c$ for $\alpha > 0$ and $a = v$ for $\alpha < 0$. For the response second order perturbation theory, it is convenient to define each of the terms appearing in Eq. (67) as

$$\widetilde{\mathcal{Q}}^{\lambda}(\mathbf{k}) = 2\pi {\rm Re}\left\{u_x u_z^*\right\} (ev_F)^2 F_\lambda(\mathbf{k}) \delta_\lambda(\omega, \mathbf{k}) \tag{69}$$

From Eq. (68), we get a map between the response tensors $\widetilde{\mathcal{Q}}^{\alpha\beta}_{kmn}(\mathbf{k})$ defined in the $k_x > 0, k_y > 0$ quadrant of the reduced Brillouin zone, to the processes corresponding to $\widetilde{\mathcal{Q}}^{\lambda}(\mathbf{k}_E)$ in Eq. (69), where $\mathbf{k}_E$ takes value in the $k_x > 0, k_y > 0$ quadrant of the extended Brillouin zone. This map is constructed such that both $\mathbf{k}_E$ and λ are functions of $\mathbf{k}$, α and β. This map is given explicitly in Table I.

Reduced zone $\widetilde{\mathcal{Q}}^{\alpha\beta}_{yxy}(\mathbf{k})$		Extended zone $\widetilde{\mathcal{Q}}^{\lambda}(\mathbf{k}_E)$	
α	β	$\mathbf{k}_E$	λ
$2n+3$	$-(2n+1)$	$\mathbf{k}+n\mathbf{q}$	$+1$
2	-1	$\mathbf{k}$	-1
$2n+1$	$-(2n+3)$	$\mathbf{k}+(n+1)\mathbf{q}$	-1
$2n+4$	$-2(n+2)$	$-\mathbf{k}+(n+1)\mathbf{q}$	$+1$
1	-2	$-\mathbf{k}+\mathbf{q}$	-1
$2n+2$	$-(2n+4)$	$-\mathbf{k}+(n+2)\mathbf{q}$	-1
$2n+1$	$-(2n+1)$	$\mathbf{k}+n\mathbf{q}$	0
$2n+2$	$-(2n+2)$	$-\mathbf{k}+(n+1)\mathbf{q}$	0

Table I: Mapping between the response tensors in the reduced Brillouin zone $\widetilde{\mathcal{Q}}^{\alpha\beta}_{yxy}(\mathbf{k})$ and the results obtained in second order perturbation theory. Only the values for the pairs (α,β) that have non zero rate in second order perturbation theory are shown. Note that the functions $\widetilde{\mathcal{Q}}^{\alpha\beta}_{yxy}(\mathbf{k})$ are defined for momenta $\mathbf{k}$ in the $k_x>0, k_y>0$ of the *reduced* Brillouin zone. The value of these functions, in second order perturbation theory, corresponds to $\widetilde{\mathcal{Q}}^{\lambda}(\mathbf{k}_E)$, where λ and k_E take the values shown in the table. In the left two columns, the n is an integer such that $n\geq 0$.